Science of the Total Environment 851 (2022) 158138

Mineralogy and fluid chemistry controls on lithium isotope fractionation during clay adsorption

Wenshuai Li, Xiao-Ming Liu *

Department of Earth, Marine and Environmental Sciences, University of North Carolina, Chapel Hill, NC, USA

HIGHLIGHTS

- We compared Li isotope fractionations during kaolinite and smectite adsorption.
- We assessed the impacts of mineralogy and fluid chemistry on isotope fractionation.
- Clay adsorption generated kinetic and equilibrium isotopic fractionations in closed system.

GRAPHICAL ABSTRACT

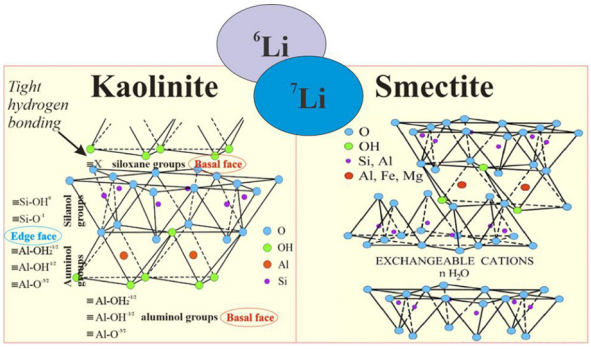

ARTICLE INFO

Editor: Xinbin Feng

Keywords:
Lithium isotopes
Experiment
Kaolinite
Smectite
Fluid chemistry
Weathering

ABSTRACT

Our current understanding of controls on δ^7Li variability and fractionation mechanisms is limited, complicating the interpretation of chemical weathering. The role of clay adsorption in Li isotope fractionation during chemical weathering has been confirmed. However, clay assemblage and fluid chemistry are not simple and often variable in weathering settings, potentially modulating Li isotope fractionation on Earth's surface. Here, this research investigated the patterns and processes of Li isotope fractionation during adsorption on kaolinite and smectite with fluid chemistry of 0.001 M NaCl, 0.5 M NaCl, and 0.001 M Na_2HPO_4. Specifically, the time-dependent experiments with the reaction period up to 15 days revealed that the steady state can be achieved within one day under neutral conditions. The concentration-dependent (initial Li concentration of 2 to 1000 μM) experiments confirmed the accumulation of Li^+ in smectite interlayers and adsorption of Li^+ only at the external surfaces of kaolinite. Using 0.5 M NaCl solution and the desorption experiments, we hypothesize that outer-sphere Li may exist in the interlayer sites, which can be replaced by excess Na^+. In comparison, inner-sphere Li^+ (unexchangeable) potentially dominates at the edge surface of clays. The presence of Na_2HPO_4 increases the binding capacity for Li^+ adsorption, in particular for kaolinite. In all cases, ^{6}Li is enriched on clay surfaces and interlayer spaces, consistent with field observations. Fluid chemistry may affect the degree of clay Li adsorption but exerted negligible impacts on isotope fractionation. For kaolinite, a wide variation (up to 30 ‰) in isotopic fractionation between adsorbed and aqueous Li ($\Delta^7Li_{aq\text{-}ad}$) exists, conforming to a kinetic fractionation mechanism with a constant fractionation factor $\alpha_{ad\text{-}aq}$ of ~0.992. By contrast, the isotopic fractionation between Li adsorbed on smectite and Li^+ left in solutions keeps constant ($\Delta^7Li_{aq\text{-}ad}$ of ~5 ‰), likely following an equilibrium isotope fractionation law with an $\alpha_{ad\text{-}aq}$ of ~0.995.

* Corresponding author.
E-mail address: xiaomliu@unc.edu (X.-M. Liu).

http://dx.doi.org/10.1016/j.scitotenv.2022.158138
Received 9 June 2022; Received in revised form 4 August 2022; Accepted 15 August 2022
Available online 17 August 2022

1. Introduction

Silicate weathering is one of the key factors controlling global climate and carbon cycles through consumption of atmospheric carbon dioxide (Berner and Berner, 1997; West et al., 2005). Incongruent silicate weathering promotes secondary clay formation as soils form, which serves as the direct evidence of weathering alteration (Tabor et al., 2002; John et al., 2003). The preferential loss of alkali elements during weathering drives the cycling of elements such as Li and K, and their stable isotopes are fractionated by weathering processes (e.g., Dellinger et al., 2015; Pogge von Strandmann et al., 2019; Li et al., 2021; Li et al., 2022).

Lithium isotopes have been used as a weathering tracer since significant Li isotope fractionations occur during chemical weathering (Huh et al., 2001; Pistiner and Henderson, 2003; Vigier et al., 2008; Millot et al., 2010; Liu et al., 2013; Dellinger et al., 2015; Pogge von Strandmann et al., 2017a; Pogge von Strandmann et al., 2017b; Hindshaw et al., 2019; Li et al., 2020; Ma et al., 2020). And it is well established that isotopically lighter Li is preferentially scavenged by clays from the aqueous solution, leaving water isotopically heavier. As a result, a wide range of Li isotope fractionation up to ~60 ‰ in the crust, water, and carbonates relative to the bulk silicate Earth and mantle was reported (e.g., Tomascak et al., 2016; Penniston-Dorland et al., 2017; Pogge von Strandmann et al., 2020). Previous studies reveal the potential of Li isotope signals in soils, sediments, river water, and past seawater to quantitively reconstruct the intensity and/or rate of chemical weathering and hydrological conditions (e.g., Misra and Froelich, 2012; Dellinger et al., 2017; Li and Liu, 2020; Xu et al., 2022; Zhang et al., 2022). To better interpret Li isotope information in geological records, the processes and mechanisms of isotopic fractionation during clay formation (adsorption and incorporation) require further investigation.

Experimental studies could provide robust constraints on the processes and mechanisms responsible for Li isotope fractionation during clay formation. Early surveys of Li adsorption on clay minerals and concomitant isotopic fractionation between reacted and initial fluids showed intriguing data, i.e., $\Delta^7Li_{\text{reacted solution-source solution}}$ of 7.7–24.8 ‰ for gibbsite, 1.6 ‰ for ferrihydrite, 7.1 ‰ for kaolinite, 3.8 ‰ for chlorite, but close to zero for montmorillonite and illite under ambient conditions (Pistiner and Henderson, 2003; Millot and Girard, 2007). Synthesis experiments of smectite by Vigier et al. (2008) reported $\Delta^7Li_{\text{fluid-clay}}$ in a range from 1.6 ‰ at 250 °C to ~10.0 ‰ at 25–90 °C, following an equilibrium isotopic fractionation mechanism. A strong kinetic control on isotope fractionation during low-temperature fluid-rock reaction has been identified in recent studies. For example, Wimpenny et al. (2015) emphasized the diffusive isotope effect during Li^+ uptake at gibbsite interlayers due to a swelling feature. Using ^{7}Li nuclear magnetic resonance (NMR), Hindshaw et al. (2019) synthesized Mg-rich layered silicates (stevensite and saponite) and estimated site-specific isotope fractionation at octahedral outer-sphere and pseudo-hexagonal sites, reflecting an interlay of equilibrium and kinetic fractionation paths. A recent study by Li and Liu (2020) confirmed the kinetic fractionation path ($\Delta\delta^7Li_{\text{aq-initial}}$ up to ~30 ‰, with an $\alpha_{\text{ad-aq}}$ ~0.992) during kaolinite adsorption that may be ascribed to an ion-desolvation process. While Li isotope fractionation directions are broadly consistent with each other, the large variability hints at mineralogy-specific isotope fractionation and fluid chemistry controls that are not yet fully understood. The mineralogy control on adsorption was emphasized by field data and modeling (Li and West, 2014; Dellinger et al., 2015; Wanner et al., 2017). However, it was only examined by Pistiner and Henderson (2003) and Millot and Girard (2007) via nonsystematic adsorption experiments. The fluid chemistry control is important considering the impact of electrolyte background on clay surface property (e.g., charge and binding site availability) (Chang et al., 2018). All of them may cause different degrees of Li isotope fractionation.

This study aims to understand the mechanisms of Li isotope fractionation during clay adsorption, focusing on the controls of clay mineralogy and fluid chemistry. In brief, the isotope compositions of adsorbed and aqueous Li were measured, and isotopic fractionation was calculated based on experimental setup using two common clay minerals (kaolinite and smectite) with varying fluid chemistry (0.001 M NaCl, 0.5 M NaCl, and 0.001 M Na_2HPO_4). The results improve the understanding of Li isotope compositions in soils, sediments, and rivers with implications to trace chemical weathering and climate change.

2. Experiment and analysis

2.1. Regents and materials

Guaranteed reagent grade acids (Fisher Scientific™) were purified using a sub-boiling Savillex™ distiller and purified water was obtained from a water purification system (Milli-Q™ Direct-Q 3UV (18.2 MΩ·cm). Smectite and kaolinite were chosen, representing major soil components driven by weathering and pedogenesis. There are marked differences between their structures. Smectite is a 2:1 layer phyllosilicate mineral, and its alumina octahedron is located between silica tetrahedron sheets. By contrast, Kaolinite is a 1:1 layer mineral, with its alumina octahedron and silica tetrahedron sheets arranged in parallel (Brigatti et al., 2006). We used well-characterized kaolinite (KGa-2) and smectite (SWy-2) sourced from the Clay Mineral Society (www.clays.org). Ultrapure NaCl and Na_2HPO_4 (>99.9 %) were purchased from Fisher Scientific™. Powdered materials were processed to recover 0.1–1 μm fraction and intensively cleaned to preclude impurities following the protocol in Li and Liu (2020) and Li et al. (2021). After cleaning, Li concentration in eluents was below the Q-ICP-MS detection limit. Prior to experiments, the control groups (water-clay mixture without initial LiCl, a duration of 15 days) were used to monitor potential Li^+ interference released from clays. And negligible Li^+ release was found (Li and Liu, 2020).

2.2. Adsorption experiment setup

We designed clay-fluid interaction experiments to assess the direction and magnitude of Li isotope fractionation during adsorption on kaolinite and smectite at the constant pH of 8 (22.5 °C) in closed systems. Before each experiment, clays were suspended in water without adding LiCl, and pH was adjusted using trace amounts of HCl or NaOH. After overnight suspension, LiCl ($\delta^7Li = 5.8 \pm 1.1$ ‰, Li and Liu, 2020) was added and well-mixed into solution. The aim of this step is to avoid large pH variation during experiments. There were slight decreases in pH at the very beginning, likely stemming from hydroxyl deprotonation and proton release due to ion exchange (Lawagon et al., 2016; Brazier et al., 2019). The pH conditions during experiments were monitored using a pH meter (Orion Sta A221) and maintained at required level. Fluctuation in pH was less than ±0.25. The solid-to-fluid ratio was fixed at 10 g/L for kaolinite and 2 g/L for smectite. Three experiment sets were designed, and the details are:

(1) Time-dependent experiments

In this experimental set, we recorded temporal change in Li concentration and isotope composition of fluids over a period of 15 days. Experiments were carried out in 250 mL acid-cleaned borosilicate Erlenmeyer flasks filled with 200 mL clay slurries with 75 μM Li and continuously stirred at 150 rpm using magnetic bars. This experimental set was designed to track temporal variation in fluid chemistry and the time to reach the steady state. During the experiment, solutions were sampled at different time intervals from the same reactor and filtrate. We infer that possible change in solid-to-fluid ratio by sampling is negligible because only small amounts of solution were collected (0.5 mL for element analysis and 2 mL for isotopic analysis). In this study, fluid chemistry was set to 0.001 M, 0.5 M NaCl, and 0.001 M Na_2HPO_4, respectively. In experiment sets, the choices of fluid chemistry were made based on general natural conditions. For example, the use of 0.001 M and 0.5 M NaCl aims to investigate the pattern of Li adsorption and isotope fractionations in low-salinity (river water in general) and high-salinity aqueous environments (e.g., seawater, brines, and groundwater in some cases, Miller et al., 1986). The use of 0.001 M Na_2HPO_4 aims to

assess the impact of widespread oxyanions (e.g., dissolved inorganic phosphate ions) in Earth's surface environments (e.g., soils, lakes, rivers and oceans) (Arai and Sparks, 2007; Nikanorov and Brazhnikova, 2009). It is recognized that oxyanions potentially exert strong impacts on clay interfacial properties (Johnston and Tombacz, 2002), but the influence on Li adsorption and corresponding isotopic fractionation remains elusive. Each experiment was performed once for each clay set.

(2) Concentration-dependent experiments

In this experimental set, we recorded the ratio of adsorption and isotopic fractionation of Li by adjusting initial Li molarity from 2 to 1000 μM. Experiments were performed in borosilicate Erlenmeyer flasks filled with 200 mL clay slurries and shaken at 150 rpm in a thermostatic water bath shaker (Thermo Scientific™ TSSWB 15) for 3 days, which was determined to reach the steady state based on data of the first experimental set). The aim is to set a wide range of adsorption ratio and degree of isotope fractionation. In addition, fluid chemistry was provided using 0.001 M NaCl, 0.5 M NaCl, and 0.001 M Na_2HPO_4 in the individual groups, respectively. We used 0.001 M and 0.5 M NaCl to represent freshwater and seawater (or brine), respectively (Li and Liu, 2020). We also used 0.001 M Na_2HPO_4, which is ~100–1000 times higher than natural river water P contents (Mainstone and Parr, 2002) to represent eutrophic (or anthropogenic) water. We used different electrolytes to assess the impacts of fluid chemistry on Li adsorption and isotopic fractionation. We performed the triplicates for individual experiments and reported the average value. The uncertainty of Li adsorption calculated from triplicates may reflect a sum of pH variations (<0.25), filtration loss (<3 %) and the one standard deviation (1 S.D.) of the Q-ICP-MS analysis (<3 %).

(3) Desorption experiments

In this experimental set, we recorded the extent of Li desorption from reacted clays in experiments with 50 μM Li and 0.001 M NaCl. This initial step was carried out in 250 mL borosilicate Erlenmeyer flasks. NH_4Ac salt was added to maintain the ionic strength (IS, provided by NH_4Ac) ranging from 0.1 M to 1 M. Reacted clays were treated with NH_4^+ exchange and continuously stirred using magnetic bars for 3 days. Desorbed Li in reacted solutions was analyzed. The aim is to determine the proportion and isotopic composition of exchangeable Li residing on the external surfaces and interlayer space.

At the end of the experiments, clay suspensions were sampled after centrifuging and rinsed by purified water. Supernatants were collected after filtration using 0.22 μm PTFE syringe filters. Filtration did not modify aqueous Li concentration for >3 % (within the analytical uncertainty of Q-ICP-MS) and Li isotope fractionation produced by filtration was undetected (using prepared LiCl solutions). Samples were transferred to centrifuge tubes and stored at 4 °C until analysis.

2.3. Elemental analysis

Samples were dissolved in 2 % HNO_3 and measured on a Q-ICP-MS (Agilent™ 7900) at the University of North Carolina at Chapel Hill. The concentrations of dissolved elements (Li, Na, K, Al, and Ca, etc.) were measured, and the instrument was calibrated using a series of ICP standards with known concentrations. Internal standards, including Be, Ge, Rh, In, Ir, and Bi were used for instrumental drift correction. Procedural blanks were undetected. In addition, two USGS standards BHVO-2 (basalt) and GSP-2 (granodiorite) were measured to ensure the analytical reproducibility with a precision of 10 % (Table 1).

2.4. Chromatography and isotope analysis

Samples were purified using a dual-column system (Liu and Li, 2019). Samples in 0.7 M HNO_3 were loaded on the first column (inside diameter: 1.5 cm), containing 17 mL AG50-X8 cation-exchange resin (200–400 mesh, Bio-Rad™). The first Li fraction was collected to eliminate the interference of most matrices including >80 % Na. Elution was evaporated to dryness and dissolved in 2 mL 0.2 M HCl. Samples were passed through the second column (ID: 0.6 cm), filled with 3.4 mL AG50-X8 resin (200–400 mesh, Bio-Rad™). To enhance total Li recovery, after cuts containing Li tails may additionally go through the same column again. Pre- and post-cuts were checked to confirm quantitative Li recovery >99 % and preclude any matrix effect for accurate Li isotope analysis. Total procedural blanks were monitored (<1 ng), and in all the cases, negligible compared with sample sizes at μg-levels.

Table 1
Inter-laboratory comparison of elemental compositions in a couple of USGS standards.

SRM NO.	Description	[Li] (ppm)
BHVO-2	Basalt, USGS,	5[a] **4.5**[b] n.d.[c] 4.3[d] 9.1[e]
GSP-2	Granodiorite, USGS,	36[a] **35.1**[b] 34.8[d]

Note:
[a] Certified values.
[b] This study.
[c] Zhao and Zheng (2015).
[d] Zhang et al. (2016).
[e] Braukmüller et al. (2018).

The $^7Li/^6Li$ ratios were measured on a Q-ICP-MS (Agilent™ 7900) at the University of North Carolina - Chapel Hill, following the method documented in Liu and Li et al. (2019). Briefly, Li in samples and standards were matrix matched to a concentration of 0.5 ppb using 2 % HNO_3. Samples were introduced using a microflow self-aspirating (Agilent™, 200 μL/min) PFA nebulizer, a quartz spray chamber, and a quartz torch. A sample-standard bracketing method was adopted and concentration matching between standards and samples was limited to >95 %. The $^7Li/^6Li$ ratio was reported in a δ notation relative to an IRMM−016 Li standard (equivalent to the L-SVEC standard), following the equation:

$$\delta^7\mathrm{Li}\ (‰) = \left\{ \frac{\left(^7\mathrm{Li}/^6\mathrm{Li}\right)_{\ \mathrm{sample}}}{\left(^7\mathrm{Li}/^6\mathrm{Li}\right)_{\ \mathrm{L-SVEC}}} - 1 \right\} \times 1000 \quad (1)$$

A long-term reproducibility from replicate measurements of international references was better than 1.1 ‰ (two standard deviations, 2 S.D.) (Liu and Li, 2019). Certified standards were analyzed, yielding δ^7Li values conform to reported reference data (Table 2): BHVO-2 (4.6 ± 1.2 ‰), GSP-2 (−0.7 ± 0.9 ‰), and NASS-7 (31.0 ± 0.9 ‰) (2 S.D.). The δ^7Li values of adsorbed Li were corrected by deducting from the original structural Li composition of clay structures (KGa-2: 0.2 ± 0.6 ‰; SWy-2: −0.6 ± 0.7 ‰) following the equation:

$$\delta^7\mathrm{Li}_{\mathrm{ad}} = \frac{[\mathrm{Li}]_{\mathrm{solid}} \times \delta^7\mathrm{Li}_{\mathrm{solid}} - [\mathrm{Li}]_{\mathrm{unreacted\ clay}} \times \delta^7\mathrm{Li}_{\mathrm{unreacted\ clay}}}{[\mathrm{Li}]_{\mathrm{ad}}} \quad (2)$$

where $[Li]_{solid}$ and δ^7Li_{solid} imply the Li concentration and isotope composition of reacted clays, respectively, and $[Li]_{unreacted\ clay}$ and $\delta^7Li_{unreacted\ clay}$ indicate the Li concentration and isotope composition of pristine (unreacted) clays, respectively. The isotope fractionation between aqueous Li and adsorbed Li ($\Delta^7Li_{aq\text{-}ad}$) was defined following the equation:

$$\Delta^7\mathrm{Li}_{\mathrm{aq-ad}} = \delta^7\mathrm{Li}_{\mathrm{aq}} - \delta^7\mathrm{Li}_{\mathrm{ad}} \quad (3)$$

where δ^7Li_{aq} and δ^7Li_{ad} imply the isotope values of aqueous and adsorbed Li, respectively.

Table 2
Inter-laboratory comparison of K isotopic compositions in serval USGS standards.

SRM NO.	Description	$\delta^7Li_{measured}$ (‰)	2 S.D. (‰)	N	Instrument
		4.6[a]	**1.2**	**6**	Q-ICP-MS
		4.6[b]	0.3	3	MC-ICP-MS
BHVO-2	Basalt, USGS	4.7[c]	0.6	7	Q-ICP-MS
		4.5[d]	0.2	4	MC-ICP-MS
		4.4[e]	0.3	8	MC-ICP-MS
		−0.7[a]	**0.9**	**6**	Q-ICP-MS
		−0.6[b]	0.6	3	MC-ICP-MS
GSP-2	Granodiorite, USGS	−0.6[c]	0.7	7	Q-ICP-MS
		−0.8[d]	0.3	5	MC-ICP-MS
		−0.8[e]	0.3	29	MC-ICP-MS
		31.0[a]	**0.9**	**6**	Q-ICP-MS
NASS-7	Seawater, NRC	30.4[b]	1	3	MC-ICP-MS
		30.6[c]	1.3	7	Q-ICP-MS

Note:
[a] This study.
[b] Li et al. (2019).
[c] Li et al. (2019).
[d] Lin et al. (2016).
[e] Sun et al. (2016).

3. Results

3.1. Characterization of Li adsorption patterns

In time-dependent experiments ([Li] of 75 μM, 0.001 M NaCl), the ratio of Li adsorbed on investigated clays ranged from 37 to 59 % (kaolinite) and 47 to 57 % (smectite). In time-dependent experiments ([Li] of 75 μM, 0.5 M NaCl), the ratio of Li adsorption ranged from 39 to 54 % (kaolinite) and 18 to 47 % (smectite). In time-dependent experiments ([Li] of 75 μM, 0.001 M Na_2HPO_4), the ratio of Li adsorption ranged from 57 to 63 % (kaolinite) and 38 to 40 % (smectite). Overall, Li adsorption ratio increased rapidly at the very beginning of experiments, and then the steady state was reached within one day (Table 3. Figs. 1a-1b), consistent with the results reported in Li and Liu (2020).

In concentration-dependent experiments ([Li] from 2 to 1000 μM) with varying fluid chemistry, the ratio of Li adsorbed on clay minerals ranged from 12 to 98 % (kaolinite) and 10 to 78 % (smectite). Li adsorption increased with decreasing initial Li molarity. Compared with Li adsorption with the addition of 0.001 M NaCl (13 to 98 %, kaolinite; 24 to 78 %, smectite), the use of 0.5 M NaCl significantly decreased Li adsorption for smectite (10 to 37.5 %) but it was not the case for kaolinite (12 to 98 %). In contrast, the presence of 0.001 M Na_2HPO_4 slightly increased the degree of Li adsorption for smectite (23–60 %, smectite) but exerted negligible impacts on kaolinite (14–95 %) (Table 4, Fig. 1c).

Clay Li coverage (adsorbed Li content divided by clay BET-N_2 surface area, kaolinite, KGa-2, 20.14 m^2/g; smectite, SWy-2, 28.60 m^2/g, Brazier et al., 2019) was calculated for direct comparison among clays (and even smectite and kaolinite). In time-dependent experiments, smectite Li coverage (0.62 to 0.74 μM/m^2) was near three times of kaolinite (0.14 to 0.22 μM/m^2) under the same condition (sampling time interval) (Table 3). In concentration-dependent experiments, smectite Li coverage ranged from 0.01 to 4.12 μM/m^2, and kaolinite Li coverage ranged from 0.01 to 0.72 μM/m^2 (Table 4). As fluid chemistry changed from 0.001 M NaCl to Na_2HPO_4, there is no distinguishable change in smectite Li coverage, but kaolinite Li coverage increases slightly. As fluid chemistry was set using 0.5 M NaCl, clay Li coverages of smectite and kaolinite with the same amount of initial LiCl were comparable. When adding more Li, clay Li coverage was higher, and the coverage plateau was not reached (Fig. 3a).

3.2. Characterization of Li isotope fractionation

In time-dependent experiments ([Li] 75 μM, 0.001 NaCl), there was an enrichment of ^6Li on clays and δ^7Li_{aq} (Li in solutions) ranged from 12.1 to 13.5 ‰ (kaolinite) and 7.4 to 8.2 ‰ (smectite). In time-dependent experiments ([Li] 75 μM, 0.05 M NaCl), δ^7Li_{aq} ranged from 10.6 to 14.1 ‰ (kaolinite) and 5.6 to 5.9 ‰ (smectite). In time-dependent experiments ([Li] 75 μM, 0.001 M Na_2HPO_4), δ^7Li_{aq} ranged from 12.1 to 13.5 ‰ (kaolinite) and 5.4 to 5.8 ‰ (smectite). The isotopic composition of aqueous Li at the very start (<1 day) can be slightly heavy and then kept constant within uncertainty (±1.1 ‰; Q-ICP-MS analysis of Li isotope data reported in this study, Liu and Li, 2019) (Table 3, Fig. 2a).

In concentration-dependent experiments ([Li] of 2–1000 μM) with the variation in fluid chemistry, δ^7Li_{aq} of the smectite group spanned a small range from 5.6 to 9.5 ‰ and that of kaolinite was relatively wide (6.2 to 35.2 ‰). Varying fluid chemistry produced no δ^7Li_{aq} difference for both clays (Table 4, Fig. 2b). Specifically, smectite δ^7Li_{aq} ranged from 5.9 to 9.5 ‰ (0.001 NaCl), 5.6 to 9.2 ‰ (0.5 M NaCl), and 7.6 to 9.4 ‰ (0.001 Na_2HPO_4), while kaolinite δ^7Li_{aq} varied from 6.2 to 33.5 ‰ (0.001 NaCl), 6.3 to 35.2 ‰ (0.5 M NaCl), and 7.6 to 29.1 ‰ (0.001 Na_2HPO_4). We also calculated δ^7Li_{ad} (adsorbed Li) by mass-balance, exhibiting a range from 2.7 to 7.9 ‰ of the kaolinite group, higher than that of the smectite group (0.6 to 4.5 ‰). At pH of 7.5, there was no significant fluid chemistry dependence of δ^7Li_{aq}. With gradual decreases in kaolinite Li coverage, the isotopic fractionation between fluid and adsorbed ($\triangle^7Li_{aq\text{-}ad}$) increased (Fig. 3b). As for smectite, $\Delta^{41}Li_{ad\text{-}aq}$ kept nearly constant (5 ‰) at pH of 7.5, despite of varying Li adsorbed concentration onto smectite at constant pH by several orders of magnitude (Fig. 3b).

With increasing Li ratio, ^6Li was preferentially removed by clays and ^7Li was enriched in solutions. The difference in isotope fractionation in response to adsorption for kaolinite and smectite was identified (Fig. 4). To reconcile the discrepancy, different mechanisms may be invoked to explain observed Li isotope fractionation. We described Li isotope fractionation as a function of adsorption ratio by batch steady-state (Eq. 4) and Rayleigh distillation (Eq. 5) equations (Fig. 4):

$$\delta^7Li_{ad} = \left(\frac{\alpha \times \delta^7Li_{LiCl} + 1000 f_{Li} \times (\alpha - 1)}{\alpha\,(1 - f_{Li}) + f_{Li}}\right); \delta^7Li_{aq} = \left(\delta^7Li_{LiCl} - f_{Li}\right)/(1 - f_{Li}) \quad (4)$$

$$\delta^7Li_{ad} = \left(\frac{\left(\delta^7Li_{LiCl} + 1000\right) \times \left(1 - (1 - f_{Li}) \times \alpha\right)}{f_{Li} - 1000}\right); \quad \delta^7Li_{aq} = e^{\left[(\alpha - 1)\ \ln f_{Li} + \ \ln\left(\delta^7Li_{LiCl} + 1000\right)\right]} - 1000 \quad (5)$$

where $\alpha_{ad\text{-}aq}$ is the isotopic fractionation factor between adsorbed Li and aqueous Li, δ^7Li_{LiCl} is the δ^7Li value of starting LiCl salt (5.8 ± 1.1 ‰), and f_{Li} denotes the fraction of Li remained in fluids while 1-f_{Li} is the proportion of Li adsorbed onto clays. This batch steady-state model in closed systems assumes continuous, fully reversible isotope exchange (Johnson et al., 2004), while the Rayleigh distillation model considers that one phase could be continuously removed from the system but is not fully reversible. We use series of isotope fractionation factor ($\alpha_{ad\text{-}aq}$) for curve fitting (Fig. 4). The results suggest that an $\alpha_{ad\text{-}aq}$ of 0.992 (kinetic, Rayleigh) provides the best fit for kaolinite experiment data, consistent with the findings of Li and Liu (2020). By contrast, an $\alpha_{ad\text{-}aq}$ of ~0.995 (equilibrium, steady-state) seems to provide the best fit for smectite experiment data.

3.3. Characterization of desorption experiments

In the desorption experiments, the initial step (50 μM Li, 0.001 M NaCl) without using NH_4Ac produced δ^7Li_{aq} of 17 ‰ after 72 % Li being adsorbed (kaolinite), and 7 ‰ after 55 % Li being adsorbed (smectite). With increments in NH_4Ac (steps I to V), Li adsorption ratio decreased from 70 to 69 % and 19 to 11 % for the kaolinite and smectite, respectively (Table 5). We note that ionic exchange of adsorbed Li^+ by NH_4^+ was

Table 3
Li adsorption and isotopic fractionation in the time-dependent experiments.

Adsorbent	Mass (g/L)	Electrolyte	T (°C)	Time (d)	Initial [Li] (μM)	Final [Li] (μM)	Adsorption (%)	$[Li]_{ad}$ [1] μM/m^2	δ^7Li_{aq} [2] (‰)
Smectite	2	1 mM NaCl	22.5	0.003	75	39.5	47.3	0.6	n.d.
	2	1 mM NaCl	22.5	0.007	75	37.7	49.8	0.7	7.4
	2	1 mM NaCl	22.5	0.014	75	36.6	51.2	0.7	n.d.
	2	1 mM NaCl	22.5	0.021	75	35.2	53.1	0.7	n.d.
	2	1 mM NaCl	22.5	0.04	75	34.2	54.4	0.7	8.2
	2	1 mM NaCl	22.5	0.12	75	33.7	55.0	0.7	n.d.
	2	1 mM NaCl	22.5	0.2	75	32.7	56.3	0.7	n.d.
	2	1 mM NaCl	22.5	0.5	75	32.5	56.6	0.7	n.d.
	2	1 mM NaCl	22.5	1	75	32.1	57.1	0.8	7.6
	2	1 mM NaCl	22.5	3	75	32.4	56.8	0.7	n.d.
	2	1 mM NaCl	22.5	7	75	32.7	56.4	0.7	n.d.
	2	1 mM NaCl	22.5	15	75	32.8	56.2	0.7	7.7
Smectite	2	0.5 M NaCl	22.5	0.003	75	39.5	17.3	0.2	n.d.
	2	0.5 M NaCl	22.5	0.007	75	37.6	19.8	0.3	5.7
	2	0.5 M NaCl	22.5	0.014	75	36.6	21.2	0.3	n.d.
	2	0.5 M NaCl	22.5	0.021	75	56.2	25.1	0.3	n.d.
	2	0.5 M NaCl	22.5	0.04	75	56.1	25.2	0.3	5.6
	2	0.5 M NaCl	22.5	0.12	75	55.7	25.7	0.3	n.d.
	2	0.5 M NaCl	22.5	0.2	75	55.9	25.4	0.3	n.d.
	2	0.5 M NaCl	22.5	0.5	75	56.0	25.3	0.3	n.d.
	2	0.5 M NaCl	22.5	1	75	55.9	25.5	0.3	5.7
	2	0.5 M NaCl	22.5	3	75	55.8	25.5	0.3	n.d.
	2	0.5 M NaCl	22.5	7	75	56.1	25.2	0.3	n.d.
	2	0.5 M NaCl	22.5	15	75	55.9	25.4	0.3	5.9
Smectite	2	1 mM Na_2HPO_4	22.5	0.003	75	46.8	37.6	0.5	5.8
	2	1 mM Na_2HPO_4	22.5	0.12	75	45.4	39.5	0.5	5.7
	2	1 mM Na_2HPO_4	22.5	1	75	45.6	39.2	0.5	5.7
	2	1 mM Na_2HPO_4	22.5	3	75	45.3	39.6	0.5	5.6
	2	1 mM Na_2HPO_4	22.5	15	75	45.5	39.4	0.5	5.4
Kaolinite	10	1 mM NaCl	22.5	0.003	75	47.0	37.3	0.1	n.d.
	10	1 mM NaCl	22.5	0.007	75	42.5	43.3	0.2	12.1
	10	1 mM NaCl	22.5	0.014	75	38.3	48.9	0.2	n.d.
	10	1 mM NaCl	22.5	0.021	75	35.7	52.4	0.2	n.d.
	10	1 mM NaCl	22.5	0.04	75	31.4	58.1	0.2	13.5
	10	1 mM NaCl	22.5	0.12	75	32.3	57.0	0.2	n.d.
	10	1 mM NaCl	22.5	0.2	75	32.2	54.1	0.2	n.d.
	10	1 mM NaCl	22.5	0.5	75	30.9	58.7	0.2	n.d.
	10	1 mM NaCl	22.5	1	75	30.9	58.9	0.2	12.4
	10	1 mM NaCl	22.5	3	75	31.6	57.9	0.2	n.d.
	10	1 mM NaCl	22.5	7	75	31.2	58.5	0.2	n.d.
	10	1 mM NaCl	22.5	15	75	30.9	58.9	0.2	12.3
Kaolinite	10	0.5 M NaCl	22.5	0.003	75	45.6	39.1	0.2	n.d.
	10	0.5 M NaCl	22.5	0.007	75	41.1	45.2	0.2	10.6
	10	0.5 M NaCl	22.5	0.014	75	39.3	47.6	0.2	n.d.
	10	0.5 M NaCl	22.5	0.021	75	38.7	48.4	0.2	n.d.
	10	0.5 M NaCl	22.5	0.04	75	35.8	52.3	0.2	14.1
	10	0.5 M NaCl	22.5	0.12	75	35.7	52.4	0.2	n.d.
	10	0.5 M NaCl	22.5	0.2	75	34.5	54.1	0.2	n.d.
	10	0.5 M NaCl	22.5	0.5	75	35.1	53.2	0.2	n.d.
	10	0.5 M NaCl	22.5	1	75	34.5	54.0	0.2	13.2
	10	0.5 M NaCl	22.5	3	75	35.3	52.9	0.2	n.d.
	10	0.5 M NaCl	22.5	7	75	35.1	53.2	0.2	n.d.
	10	0.5 M NaCl	22.5	15	75	34.1	54.5	0.2	12.7
Kaolinite	10	1 mM Na_2HPO_4	22.5	0.003	75	32.0	57.3	0.2	12.1
	10	1 mM Na_2HPO_4	22.5	0.12	75	28.4	62.1	0.2	13.3
	10	1 mM Na_2HPO_4	22.5	1	75	28.1	62.5	0.2	13.5
	10	1 mM Na_2HPO_4	22.5	3	75	27.8	63.0	0.2	13.2
	10	1 mM Na_2HPO_4	22.5	15	75	28.1	62.6	0.2	13.4

Note: n.d. means not determined. Long-term analytical uncertainty (2 S.D.) of 1.1 ‰ (Liu and Li, 2019) is used as the error of Li isotope composition, in accord with Li and Liu (2020) and Li et al. (2020).

[1] Sorbed Li on clay surfaces, $[Li]_{ad} = [Li]_{initial}\text{-}[Li]_{final})/(Mass_{clay}\cdot BET_{clay})$; The BET-$N_2$ specific surface areas of kaolinite (KGa-2, 20.14 m^2/g) and smectite (SWy-2, 28.60 m^2/g) were reported in Brazier et al. (2019) and used in this study to calculate clay K coverage.

[2] Isotopic composition of Li left in solutions.

marked for smectite while negligible for kaolinite. The difference in δ^7Li_{aq} between each step was unresolvable within the analytical error (2 S.D. = 1.1 ‰, Liu and Li, 2019). It is possible that 1) smectite Li adsorption causes no isotopic fractionation, or 2) the degree of isotopic fractionation after ~11 to 55 % Li being adsorbed by smectite is smaller than or comparable to the analytical uncertainty.

4. Discussion

Our experimental results indicate that isotopically heavy Li can be preferentially retained in solutions. Two features can be summarized: 1) the steady state of Li adsorption and isotopic fractionation can be reached within one day, and 2) the percentage of clay Li adsorption and the

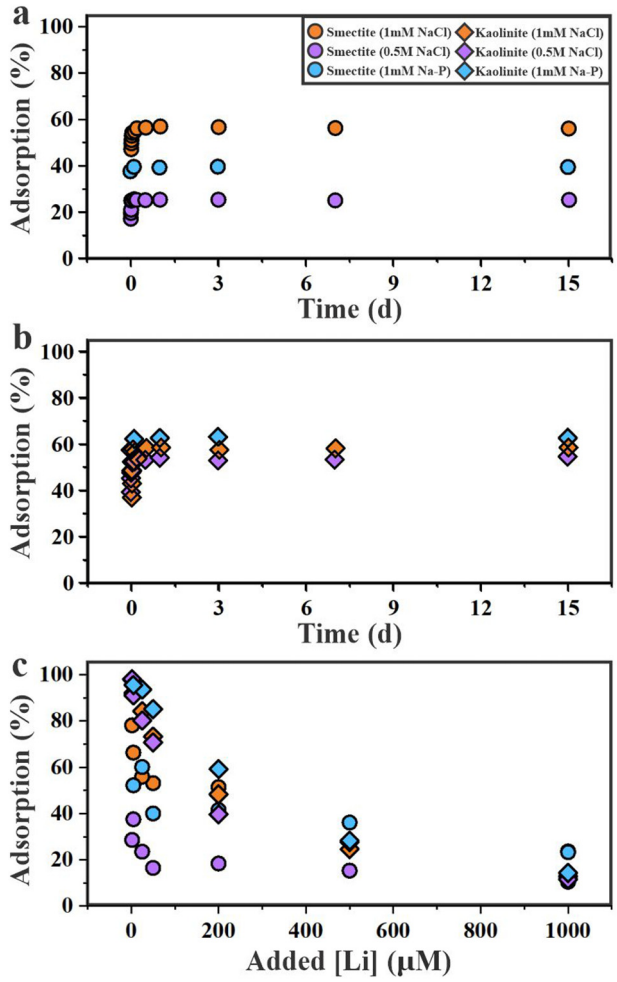

Fig. 1. Characterization of Li adsorption in time-dependent experiments of (a) smectite (added [Li] 75 μM, pH = 7.5, 0.001 M NaCl, 0.5 M NaCl, and 0.001 M Na_2HPO_4) and (b) kaolinite (added [Li] 75 μM, pH = 7.5, 0.001 M NaCl, 0.5 M NaCl, and 0.001 M Na_2HPO_4). (c) Concentration-dependent experiments ([Li] 2 to 1000 μM, pH = 7.5, fluid chemistry: 0.001 M NaCl, 0.5 M NaCl, and 0.001 M Na_2HPO_4). The Li adsorption percentage was calculated based on the ratio of Li removed from initial LiCl solutions. The error bars on the Y-axis show the 2 S.D. of the adsorption experiment triplicates. Diamonds and circles imply kaolinite and smectite groups, respectively. Colors of orange, purple and blue denote different fluid chemistry.

magnitude of Li isotope fractionation depend on mineralogy and fluid chemistry. There is an ^7Li enrichment in solutions at the start of reaction relative to solutions sampled in the later stages (Fig. 2a). This may be caused by ion diffusion with preferential transfer of lighter ^6Li from water to clay surfaces, resulting in isotopically heavier Li left in fluids. It is important to note that Zhang et al. (2022) reported a similar pattern, but a prolonged Li isotope fractionation period (days to months) based on seasonal river data and loess dissolution experiments (potentially including interrelated dissolution, clay formation/transformation, and adsorption). A recent study highlighted the dominance of water residence time in controlling riverine Li isotope composition (Zhang et al., 2022), similar to conclusions of previous riverine and groundwater Li isotope studies in catchment and global scales (Wanner et al., 2014; Liu et al., 2015;). We suggest that this study only provides a simplified situation, i.e., Li adsorption on clays without considering other coinstantaneous weathering processes, while dynamic weathering system generally needs more time to reach the steady state. After reaching the steady state in the experiments, the isotopic fractionation between aqueous and adsorbed Li is up to ~30 ‰ for kaolinite following the kinetic isotope fractionation mechanism (Fig. 4). By contrast, a small and constant isotopic fractionation for smectite is likely driven by the equilibrium isotope fractionation mechanism (Fig. 4). The results suggest the importance of both kinetic and equilibrium Li isotope fractionation during chemical weathering and clay formation.

4.1. Mineralogy control

There is a strong mineralogy control on Li isotope fractionation during clay adsorption. Combined with the results of this study and Li and Liu (2020), the variability in calculated $\Delta^7Li_{aq\text{-}ad}$ value of the kaolinite group is significant (~30 ‰) relative to that of the smectite group, which is homogeneous (~5 ‰, Fig. 3b). Given this difference, we propose that the mechanisms of Li isotopic fractionation are distinct for kaolinite (kinetic) and smectite (equilibrium) based on the isotope model fitting (Fig. 4). We hypothesize that inner-sphere complexed Li on kaolinite dominate in this study, which can be supported by two lines of evidence. First, we found similar Li adsorption patterns using limited (0.001 M) and excess (0.5 M) Na^+, respectively (Fig. 1) in consideration of ionic replacement of exchangeable Li^+ with excess Na^+. Second, pre-adsorbed Li^+ on kaolinite is unexchangeable and isotopic fractionation keeps near constant during the desorption experiments with NH_4Ac. Li and Liu (2020) has also suggested that exchangeable Li^+ at pH > 7 is absent during kaolinite Li adsorption experiments in a range of pH (4–10) and low/high ionic strength (set by NaCl). The inner-sphere complexion on the clay edge surface may be linked to silanol (≡Si-OH), aluminol (≡Al-OH), silica-alumina bridging sites (≡Si/Al-OH), or alumina-alumina bridging (≡Al_2–OH) sites, all of which cannot be easily replaced by excess Na^+ (Bickmore et al., 2003; Tournassat et al., 2004). Zhang et al. (2021) inferred that Li onto kaolinite could be bounded to kaolinite AlO_6 edge sites in a form of octahedral inner-sphere surface complexes. There is a lack of robust evidence of octahedral inner-sphere Li on clays and further verification is necessary. We infer that the kinetic isotope fractionation is caused by inner-sphere complexes formed at the edge surface of kaolinite. In addition, Li and Liu (2020) proposed Li rapid occupation at the defect sites or diffusion into deep vacancies after ion-dehydration at the edge surfaces, which are not fully exchangeable. We hypothesize that adsorption of Li on kaolinite in forms of inner-sphere complexes at pH > 7 induces kinetic isotopic fractionation. It is important to note that the presence of inner-sphere and outers-sphere Li is only a speculation based on its exchangeable ability, which has been advocated for the adsorption of metal ions on clays using similar methods. However, direct spectroscopic evidence of Li (e.g., NMR and X-ray absorption spectroscopy) is lack because adsorbed Li on studied clays is under the spectroscopic detection limit and further investigations using advanced techniques may be needed.

As for smectite, we infer that outer-sphere complexation likely dominates Li adsorption, which causes equilibrium isotope fractionation, which is supported by the following lines of evidence. First, dissolved cations can present at the interlayer space of smectite because of higher cation exchange capacity of smectite (SWy-2, 76.4 meq/100 g) relative to kaolinite (KGa-2, 3.3 meq/100 g), despite of limited differences in external surface areas (31.82 ± 0.22 m^2/g vs. 23.50 ± 0.06 m^2/g) (CMS, www.clays.org). Second, clay Li coverages of smectite are about 3 times higher than those of kaolinite with limited Na^+ (0.001 M) at pH = 7.5 (Table 4). Relatively large specific surface area and the occurrence of interlayer space of smectite likely results in Li adsorption capacity higher than kaolinite. Under conditions with excess Na^+ (0.5 M NaCl), smectite Li coverages drop dramatically, while the surface Li loads of smectite and kaolinite are comparable under the same condition (Table 4). Therefore, we suggest that the dominance of fully exchangeable Li^+ in smectite interlayer space potentially causes the overall pattern of equilibrium isotopic fractionation.

A general rule of the equilibrium isotope fractionation is that heavier isotopes prefer to concentrate in species with stiffer bonds (Schauble, 2004). However, there is no change in the coordination number between outer-sphere complexed (exchangeable) Li and free Li^+ (N = 4, Rempe et al., 2000; Lyubartsev et al., 2001). We consider that slight distortion in the bond length and angle for outer-sphere $Li{\cdot}(H_2O)_4^+$ is possible. This is

Table 4
Li adsorption and isotopic fractionation in the concentration-dependent experiments.

Adsorbent	Mass (g/L)	Electrolyte	Initial [Li] (μM)	Final [Li] (μM)	Adsorption (%)	$[Li]_{ad}$ [1] μM/m^2	δ^7Li_{aq} [2] (‰)	δ^7Li_{ad} [3] (‰)
Smectite	2	1 mM NaCl	1000	764.4 (29.1)	23.6 (3.0)	4.12 (0.53)	5.9	n.d.
	2	1 mM NaCl	500	319.3 (7.7)	36.1 (1.5)	3.16 (0.14)	6.2	n.d.
	2	1 mM NaCl	200	97.2 (10.1)	51.4 (5.1)	1.80 (0.18)	6.4	0.6
	2	1 mM NaCl	50	23.4 (2.2)	53.1 (4.4)	0.46 (0.04)	6.5	n.d.
	2	1 mM NaCl	25	11.0 (0.3)	55.9 (1.2)	0.24 (0.01)	6.5	1.9
	2	1 mM NaCl	5	1.7 (0.3)	66.3 (5.2)	0.06 (0.00)	8.2	n.d.
	2	1 mM NaCl	2	0.4 (0.1)	78.1 (5.1)	0.03 (0.00)	9.5	2.8
	2	0.5 M NaCl	1000	894.9 (5.5)	10.5 (0.6)	0.94 (0.10)	5.8	n.d.
	2	0.5 M NaCl	500	423.4 (2.8)	15.3 (0.6)	0.74 (0.05)	5.7	n.d.
	2	0.5 M NaCl	200	162.2 (9.8)	18.4 (4.9)	0.64 (0.17)	6.2	0.6
	2	0.5 M NaCl	50	41.7 (1.6)	16.5 (3.3)	0.14 (0.03)	5.6	n.d.
	2	0.5 M NaCl	25	19.1 (2.3)	23.5 (9.3)	0.10 (0.04)	8.4	2.3
	2	0.5 M NaCl	5	3.1 (0.7)	37.5 (13.7)	0.03 (0.01)	9.2	n.d.
	2	0.5 M NaCl	2	1.4 (0.2)	28.6 (11.2)	0.01 (0.00)	8.3	3.7
	2	1 mM Na_2HPO_4	1000	767.5 (40.8)	23.3 (4.1)	4.06 (0.71)	7.6	n.d.
	2	1 mM Na_2HPO_4	500	319.6 (39.9)	36.1 (8.0)	3.15 (0.7)	8.5	n.d.
	2	1 mM Na_2HPO_4	200	117.0 (9.1)	41.5 (4.6)	1.45 (0.16)	8.4	4.5
	2	1 mM Na_2HPO_4	50	30.0 (2.5)	40.0 (5.0)	0.35 (0.04)	8.7	n.d.
	2	1 mM Na_2HPO_4	25	10.0 (1.9)	60.1 (7.5)	0.26 (0.03)	9.2	n.d.
	2	1 mM Na_2HPO_4	5	2.4 (0.4)	52.2 (7.5)	0.05 (0.01)	9.4	4.1
Kaolinite	10	1 mM NaCl	1000	872.6 (14.0)	12.8 (1.4)	0.72 (0.07)	6.2	n.d.
	10	1 mM NaCl	500	377.0 (52.9)	24.6 (10.6)	0.61 (0.26)	6.6	n.d.
	10	1 mM NaCl	200	103.5 (8.0)	48.3 (4.0)	0.48 (0.04)	9.8	2.7
	10	1 mM NaCl	50	13.4 (1.4)	73.2 (2.9)	0.18 (0.01)	17.2	n.d.
	10	1 mM NaCl	25	3.9 (0.2)	84.2 (0.6)	0.10 (0.00)	17.6	4.6
	10	1 mM NaCl	5	0.4 (0.2)	92.0 (4.1)	0.02 (0.00)	24.5	n.d.
	10	1 mM NaCl	2	0.0 (0.0)	98.0 (0.1)	0.01 (0.00)	33.5	7.9
	10	0.5 M NaCl	1000	884.2 (41.9)	11.6 (4.2)	0.61 (0.21)	6.3	n.d.
	10	0.5 M NaCl	500	361.8 (32.8)	27.6 (6.6)	0.69 (0.16)	6.5	n.d.
	10	0.5 M NaCl	200	120.8 (14.2)	39.6 (7.1)	0.39 (0.07)	9.7	2.8
	10	0.5 M NaCl	50	14.7 (4.0)	70.7 (8.1)	0.18 (0.02)	16.2	n.d.
	10	0.5 M NaCl	25	4.9 (0.6)	80.2 (2.3)	0.10 (0.00)	17.2	3.4
	10	0.5 M NaCl	5	0.4 (0.1)	91.1 (1.5)	0.02 (0.00)	22.5	n.d.
	10	0.5 M NaCl	2	0.0 (0.0)	98.1 (0.3)	0.01 (0.00)	35.2	7.3
	10	1 mM Na_2HPO_4	1000	857.0 (63.6)	14.3 (6.4)	0.71 (0.32)	7.6	n.d.
	10	1 mM Na_2HPO_4	500	358.3 (13.8)	28.3 (2.8)	0.70 (0.07)	7.9	n.d.
	10	1 mM Na_2HPO_4	200	81.5 (5.8)	59.2 (8.5)	0.59 (0.03)	13.6	2.8
	10	1 mM Na_2HPO_4	50	7.4 (0.6)	85.1 (1.3)	0.21 (0.00)	18.2	n.d.
	10	1 mM Na_2HPO_4	25	1.6 (0.3)	93.6 (1.1)	0.12 (0.00)	24.8	n.d.
	10	1 mM Na_2HPO_4	5	0.2 (0.1)	95.5 (1.5)	0.02 (0.00)	29.1	6.7

Note: n.d. means not determined. Long-term analytical uncertainty (2 S.D.) of 1.1 ‰ (Liu and Li, 2019) is used as the error of Li isotope composition, in accord with Li and Liu (2020) and Li et al. (2020). The errors (2 S.D.) in the parentheses were calculated based on the results of three sets of parallel experiments (triplicates).

[1] Amount of Li sorbed on clay surfaces, $[Li]_{ad} = [Li]_{initial}\text{-}[Li]_{final})/(Mass_{clay}\cdot BET_{clay})$; The BET-$N_2$ specific surface areas of kaolinite (KGa-2, 20.14 m^2/g) and smectite (SWy-2, 28.60 m^2/g) were reported in Brazier et al. (2019) and used in this study to calculate clay K coverage.

[2] Isotopic composition of Li left in solutions.

[3] Isotopic composition of Li adsorbed on clays.

because water molecules bind to metal ions primarily through ion-dipole bonds with electrostatic features (Persson, 2010), which could be affected by surface charge. Free Li^+ in surrounding water enriched in heavier Li potentially form stiffer Li—O bonds than surface exchangeable Li^+. This may explain small isotopic fractionation between aqueous Li^+ and exchangeable Li ($\Delta^7Li_{aq\text{-}ad}$ of ~5 ‰) for smectite (Fig. 3b and Fig. 4). The isotopic fractionation between fluids and exchangeable Li (~0 to 12 ‰) was also found in previous experimental and field studies (Chan and Hein 2007; Wimpenny et al., 2015; Hindshaw et al., 2019; Pogge von Strandmann et al., 2019). In addition, isotopic fractionation associated with outer-sphere complexation has also been observed in other isotope systems, such as Zn, Ca, Ni and Se (Guinoiseau et al., 2016; Brazier et al., 2019; Alvarez et al., 2020; Xu et al., 2020; Xu et al., 2021). Although no robust interpretation on isotope fractionation driven by outer-sphere complexation can be drawn, we infer that the charge-related process may be the case of equilibrium isotope fractionation for smectite (Fig. 4).

4.2. Fluid chemistry influence

Here, we evaluate the fluid chemistry control on the mechanism of clay Li adsorption and isotope fractionation. Increasing NaCl from 0.001 M to 0.5 M, there is limited change in kaolinite Li adsorption and isotope composition in water within analytical errors (Table 4). In comparison, a dramatic reduction occurs in smectite Li adsorption by up to ~50 % when the fluid chemistry changes from 0.001 M to 0.5 M NaCl (Fig. 1b) without distinguishable changes in δ^7Li_{aq} (<2 ‰ or less) (2. S.D. = 1.1 ‰) (Fig. 2b). Dramatic decrease in smectite Li adsorption may be caused by (i) excess Na^+ replacing Li^+ at clay interlayer spaces, and (ii) limited the access of Li^+ to the interlayer space due to clay aggregation caused by excess Na^+ (Garcia-Garcia et al., 2009). We note that negligible changes in δ^7Li_{aq} for smectite by adjusting NaCl from 0.5 M to 0.001 M do not preclude determined equilibrium isotopic fractionation ($\alpha_{ad\text{-}aq}$ of ~0.995) in Fig. 4. The main reason is that the changes in Li adsorption ratio from ~50 % to 10 % for smectite can only cause δ^7Li_{aq} difference about 2 ‰, comparable to the analytical uncertainty (2. S.D. = 1.1 ‰, the difference between the upper and lower limits is 2.2 ‰). This is also the case in the desorption experiments that the reduction in smectite Li adsorption from ~50 % to 10 % by NH4Ac extraction occurred without marked isotopic fractionation (Table 5). We note that a small portion of Li removed by smectite cannot be fully exchanged by Na^+ (0.5 M, Table 4) or NH_4^+ (0.1 to 1 M, Table 5). Rather, we hypothesize that a small number of inner-sphere Li complexes may form at smectite edge surfaces. Supportively, Bourg et al.

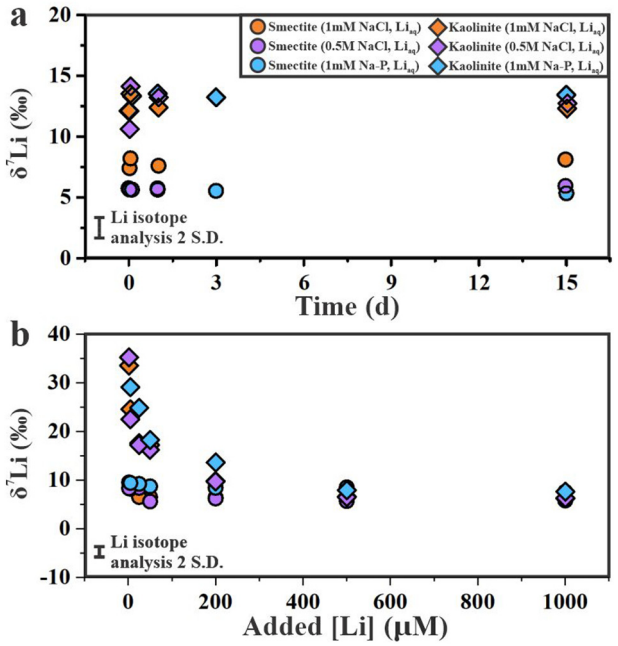

Fig. 2. Characterization of Li isotopic composition of aqueous Li in (a) time-dependent experiments (added [Li] 75 μM, pH = 7.5, fluid chemistry: 0.001 M NaCl, 0.5 M NaCl, and 0.001 M Na_2HPO_4), and (b) concentration-dependent experiments (added [Li] 2 to 1000 μM, pH = 7.5, fluid chemistry: 0.001 M NaCl, 0.5 M NaCl, and 0.001 M Na_2HPO_4). The error bars on the Y-axis show the long-term 2 S.D. of isotope analysis (1.1 ‰, Liu and Li, 2019). The error bars of Li isotopes are not shown here because they are smaller than the symbols. Diamonds and circles denote the kaolinite and smectite groups, respectively. Colors of orange, purple and blue denote different electrolytes.

(2007) suggested that alumina-alumina bridging (≡Al_2–OH) ligand is probably the most important adsorption site of smectite within the pH range of 4.5 to 9, which covers our studied pH of 7.5. However, a robust interpretation on the isotope fractionation mechanism of inner-sphere Li^+ on smectite cannot be provided due to low Li adsorption (<40 %) for fitting, making it difficult to evaluate which isotope model (Rayleigh vs. batch) provides better fits (Fig. 4).

Once the fluid chemistry changes from 0.001 M NaCl to Na_2HPO_4, there is a slight increase in the percentage of Li adsorption on kaolinite with the same initial [Li] (Table 4). By contrast, the variations in smectite Li adsorption and isotope fractionation on the surfaces of clays are limited. It is known that a small amount of positive variable charges can be generated due to the protonation of hydroxyls (≡M–OH_2^+) at the clay edge at pH of 7.5 (Manning and Goldberg, 1997; Gu et al., 2010). However, these sites are generally unavailable for Li bonding because of electrostatic repulsion. Nevertheless, the presence of HPO_4^{2-} may affect ionic exchange on kaolinite that the connection between hydroxyls and Li^+ might be bridged by HPO_4^{2-} (Olu-Owolabi and Unuabonah, 2011), providing more sites for binding. Phosphate-bridged Li^+ may induce negligible isotopic fractionation given kaolinite adsorption ratio increases without changing δ^7Li_{aq} in any group (Table 4). In comparison, the contribution of the bridge effect (ionic association between adsorbed Li and clay binding sites connected by HPO_4^{2-}) is minor for smectite, potentially because that Li^+ is mainly hosted within the interlayers as outer-sphere complexes, and the permanent negative charge of the interlayers prohibits the access of HPO_4^{2-}, thus limiting the bridging effect.

4.3. Implications for tracing chemical weathering

As chemical weathering is typically incongruent, soils form during pedogenesis, and serve as the direct evidence of continental weathering over geological time (Tabor et al., 2002; John et al., 2003). Climate change potentially affects the formation and transformation of clay mineralogy. For example, unconsolidated materials could be replaced by kaolin-group minerals (kaolinite and halloysite), and authigenic Al and Fe (oxy)hydroxides (e.g., gibbsite, ferrihydrite, and goethite) in relatively warm and humid environments (Velde and Meunier, 2008), usually featured by intense weathering. In comparison, the montmorillonite group mostly exists in hot, semi-arid and seasonally contrasted environments, particularly flooding seasons with large amounts of porewater retains in soils during dry seasons (Velde and Meunier, 2008). Longer water residence times leads to the stabilization of montmorillonite (Curtis, 1990). Because the mechanisms and degrees of Li isotope fractionation during adsorption onto kaolinite and smectite can be different based on this study, clay mineralogical difference likely yields distinct δ^7Li values in soils and pore water, and eventually in river water, groundwater and seawater. Interestingly, clay synthesis experiments indicated that Li isotope fractionation via structural incorporation is more sensitive to the

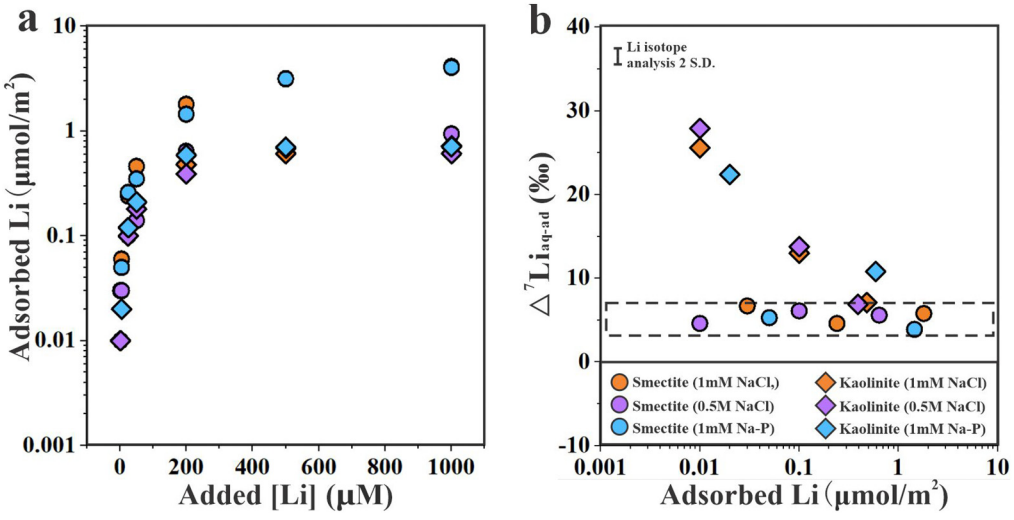

Fig. 3. (a) Clay Li coverage as a function of added [Li] at constant pH = 7.5, and (b) net Li isotope fractionation between aqueous and adsorbed Li, based on data of concentration-dependent experiments. Clay coverage was calculated from adsorbed Li content divided by BET-N_2 specific surface areas of kaolinite (KGa-2, 20.14 m^2/g) and smectite (SWy-2, 28.69 m^2/g), respectively (Brazier et al., 2019). The error bars of Li isotopes are not shown because they are smaller than the symbols. Data in the dashed box denote constant $\triangle^7Li_{aq-ad}$ of ~5 ‰ for smectite.

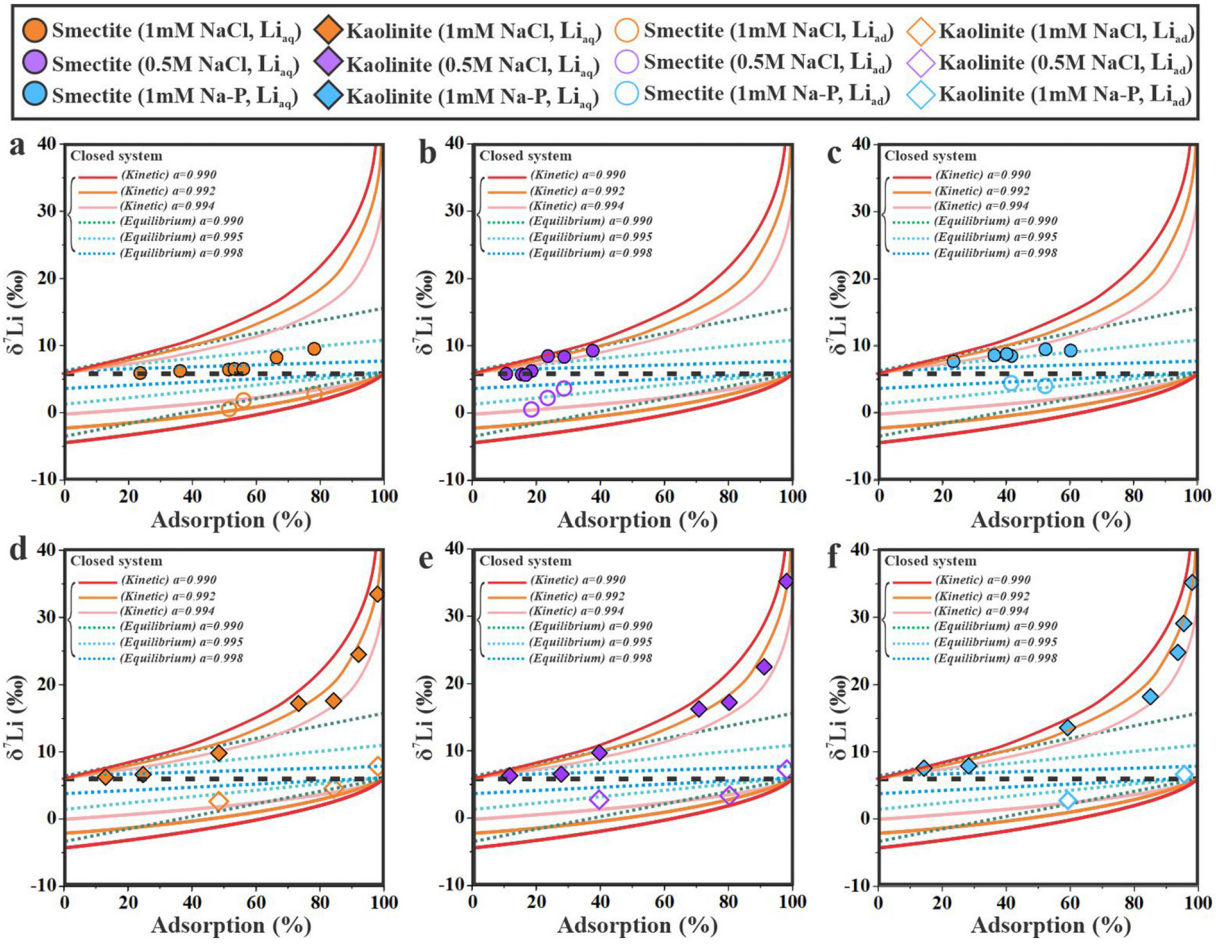

Fig. 4. The fitting of the Rayleigh distillation model (solid lines, kinetic) and batch model (dotted lines, equilibrium) in closed systems of Li isotope data for kaolinite and smectite based on concentration-dependent experiments. Filled and hallow symbols denote the data of aqueous and adsorbed Li. Colors of orange, purple and blue imply different fluid chemistry. The error bars of Li isotopes are not shown here because they are smaller than the symbols. Dashed lines denote the δ^7Li (5.8 ± 1.1 ‰) of initial LiCl salt.

atomic coordination environment, instead of solution chemistry nor the type of clay mineral formed (Vigier et al., 2008; Hindshaw et al., 2019). Therefore, the influence of clay mineralogy on δ^7Li at Earth surfaces needs to be evaluated further by comparing relative contributions of adsorption and incorporation.

5. Conclusions

This study reported experimental results of Li isotope fractionation during adsorption onto kaolinite and smectite in closed systems with varying fluid chemistry (0.001 M NaCl, 0.5 M NaCl, and 0.001 M Na_2HPO_4).

Table 5
Li adsorption and isotopic fractionation in the desorption experiments.

Adsorbent	Mass (g/L)	Electrolyte	pH	T (°C)	Step[1]	Initial [Li] (μM)[2]	Final [Li][3] (μM)	Adsorption[4] (%)	δ^7Li_{aq}[5] (‰)
	2	1 mM NaCl	8	22.5	Initial	50	22.7	54.6	7.2
	2	0.1 M NH_4Ac	8	22.5	I	0	40.4	19.2	5.3
Smectite	2	0.2 M NH_4Ac	8	22.5	II	0	42.9	14.3	6.7
	2	0.5 M NH_4Ac	8	22.5	III	0	44.7	10.7	5.9
	2	1 M NH_4Ac	8	22.5	IV	0	44.7	10.6	6.5
	10	1 mM NaCl	8	22.5	Initial	50	14.2	71.6	16.8
	10	0.1 M NH_4Ac	8	22.5	I	0	14.7	70.7	17.2
Kaolinite	10	0.2 M NH_4Ac	8	22.5	II	0	15.4	69.3	16.9
	10	0.5 M NH_4Ac	8	22.5	III	0	15.4	69.3	17.3
	10	1 M NH_4Ac	8	22.5	V	0	15.4	69.3	17.2

Note:
[1] Initial step denotes the adsorption experiments and steps I to V represent desorption experiments using NH_4Ac.
[2] LiCl was only added in the initial adsorption step.
[3] Li left in solutions including free Li^+ and a sum of desorbed Li.
[4] The extent of Li removal from initial LiCl solution.
[5] Isotopic composition of Li left in solutions (Long-term analytical uncertainty, 2 S.D. of 1.1 ‰, Liu and Li, 2019).

According to the results from time-dependent, concentration-dependent and desorption experiments, we hypothesize that inner-sphere complexes probably dominate at clay edge surfaces (especially for kaolinite) under neutral conditions, driving kinetic isotopic fractionation with a fractionation factor ($\alpha_{ad\text{-}aq}$) ~ 0.992. By contrast, outer-sphere complexes may dominate at smectite interlay spaces, producing equilibrium isotopic fractionation with a fractionation factor ($\alpha_{ad\text{-}aq}$) of ~0.995. Changing fluid chemistry mostly affected the amount of Li adsorption onto clays with negligible effects on Li isotope fractionation mechanisms. In sum, we highlight that both kinetic and equilibrium paths may be responsible for observed δ^7Li variations on Earth's surface during chemical weathering.

CRediT authorship contribution statement

Wenshuai Li: Conceptualization, sampling, Data curation, Analysis, Investigation, Methodology, Visualization, Writing. Xiao-Ming Liu: Conceptualization, Funding acquisition, Investigation, Methodology, Validation, Writing.

Data availability

Data will be made available on request.

Declaration of competing interest

The authors declare that they have no known competing financial interests or personal relationships that could have appeared to influence the work reported in this paper.

Acknowledgements

The authors acknowledge funding supports from the NSF Career Award (EAR-1848153) to X.-M. Liu and the Martin Research Fellowship at the University of North Carolina, Chapel Hill to W.-S. Li.

References

Alvarez, C.C., Quitté, G., Schott, J., Oelkers, E.H., 2020. Experimental determination of Ni isotope fractionation during Ni adsorption from an aqueous fluid onto calcite surfaces. Geochim. Cosmochim. Acta 273, 26–36.
Arai, Y., Sparks, D.L., 2007. Phosphate reaction dynamics in soils and soil components: a multiscale approach. Adv. Agron. 94, 135–179.
Berner, R.A., Berner, E.K., 1997. Silicate weathering and climate. Tectonic Uplift And Climate Change. Springer, Boston, MA.
Bickmore, B.R., Rosso, K.M., Nagy, K.L., Cygan, R.T., Tadanier, C.J., 2003. Ab initio determination of edge surface structures for dioctahedral 2: 1 phyllosilicates: implications for acid-base reactivity. Clays Clay Miner. 51, 359–371.
Bourg, I.C., Sposito, G., Bourg, A.C., 2007. Modeling the acid–base surface chemistry of montmorillonite. J. Colloid Interface Sci. 312, 297–310.
Braukmüller, N., Wombacher, F., Hezel, D.C., Escoube, R., Münker, C., 2018. The chemical composition of carbonaceous chondrites: implications for volatile element depletion, complementarity and alteration. Geochim. Cosmochim. Acta 239, 17–48.
Brazier, J.M., Schmitt, A.D., Gangloff, S., Pelt, E., Chabaux, F., Tertre, E., 2019. Calcium isotopic fractionation during adsorption onto and desorption from soil phyllosilicates (kaolinite, montmorillonite and muscovite). Geochim. Cosmochim. Acta 250, 324–347.
Brigatti, M.F., Galan, E., Theng, B.K.G., 2006. Structures and mineralogy of clay minerals. Dev. Clay Sci. 1, 19–86.
Chan, L.H., Hein, J.R., 2007. Lithium contents and isotopic compositions of ferromanganese deposits from the global ocean. Deep Sea Res. Part II Top. Stud. Oceanogr. 54 (11-13), 1147–1162.
Chang, Z., Chen, X., Peng, Y., 2018. The adsorption behavior of surfactants on mineral surfaces in the presence of electrolytes–a critical review. Miner. Eng. 121, 66–76.
Curtis, C.D., 1990. Aspects of climatic influence on the clay mineralogy and geochemistry of soils, palaeosols and clastic sedimentary rocks. J. Geol. Soc. 147, 351–357.
Dellinger, M., Gaillardet, J., Bouchez, J., Calmels, D., Louvat, P., Dosseto, A., Gorge, C., Alanoca, L., Maurice, L., 2015. Riverine Li isotope fractionation in the Amazon River basin controlled by the weathering regimes. Geochim. Cosmochim. Acta 164, 71–93.
Dellinger, M., Bouchez, J., Gaillardet, J., Faure, L., Moureau, J., 2017. Tracing weathering regimes using the lithium isotope composition of detrital sediments. Geology 45, 411–414.
Garcia-Garcia, S., Wold, S., Jonsson, M., 2009. Effects of temperature on the stability of colloidal montmorillonite particles at different pH and ionic strength. Appl. Clay Sci. 43, 21–26.
Gu, X., Evans, L.J., Barabash, S.J., 2010. Modeling the adsorption of Cd (II), Cu (II), Ni (II), Pb (II) and Zn (II) onto montmorillonite. Geochim. Cosmochim. Acta 74, 5718–5728.
Guinoiseau, A., Gélabert, J., Moureau, P., Louvat, Benedetti, M.F., 2016. Zn isotope fractionation during sorption onto kaolinite. Environ. Sci. Technol. 50, 1844–1852.
Hindshaw, R.S., Tosca, R., Goût, T.L., Farnan, I., Tosca, N.J., Tipper, E.T., 2019. Experimental constraints on Li isotope fractionation during clay formation. Geochim. Cosmochim. Acta 250, 219–237.
Huh, Y., Chan, L.H., Edmond, J.M., 2001. Lithium isotopes as a probe of weathering processes: Orinoco River. Earth Planet. Sci. Lett. 194, 189–199.
John, C.M., Mutti, M., Adatte, T., 2003. Mixed carbonate-siliciclastic record on the North African margin (Malta)-coupling of weathering processes and mid Miocene climate. Geol. Soc. Am. Bull. 115, 217–229.
Johnson, C.M., Beard, B.L., Albarède, F., 2004. Overview and general concepts. Rev. Mineral. Geochem. 55, 1–24.
Lawagon, C.P., Nisola, G.M., Mun, J., Tron, A., Torrejos, R.E.C., Seo, J.G., Kim, H., Chung, W.J., 2016. Adsorptive Li+ mining from liquid resources by H2TiO3: equilibrium, kinetics, thermodynamics, and mechanisms. J. Ind. Eng. Chem. 35, 347–356.
Li, G., West, A.J., 2014. Evolution of Cenozoic seawater lithium isotopes: coupling of global denudation regime and shifting seawater sinks. Earth Planet. Sci. Lett. 401, 284–293.
Li, W., Liu, X.M., 2020. Experimental investigation of lithium isotope fractionation during kaolinite adsorption: implications for chemical weathering. Geochim. Cosmochim. Acta 284, 156–172.
Li, W., Liu, X.M., Godfrey, L.V., 2019. Optimisation of lithium chromatography for isotopic analysis in geological reference materials by MC-ICP-MS. Geostand. Geoanal. Res. 43, 261–276.
Li, W., Liu, X.M., Chadwick, O.A., 2020. Lithium isotope behavior in Hawaiian regoliths: soil-atmosphere-biosphere exchanges. Geochim. Cosmochim. Acta 285, 175–192.
Li, W., Liu, X.M., Hu, Y., Teng, F.Z., Hu, Y., 2021. Potassium isotopic fractionation during clay adsorption. Geochim. Cosmochim. Acta 304, 160–177.
Li, W., Liu, X.M., Hu, Y., Teng, F.Z., Chadwick, O.A., 2022. Potassium isotope fractionation during chemical weathering in humid and arid Hawaiian regoliths. Geochim. Cosmochim. Acta 333, 39–55.
Lin, J., Liu, Y., Hu, Z., Yang, L., Chen, K., Chen, H., Zong, K., Gao, S., 2016. Accurate determination of lithium isotope ratios by MC-ICP-MS without strict matrix-matching by using a novel washing method. J. Anal. At. Spectrom. 31, 390–397.
Liu, X.M., Li, W., 2019. Optimization of lithium isotope analysis in geological materials by quadrupole ICP-MS. J. Anal. At. Spectrom. 34, 1708–1717.
Liu, X.M., Rudnick, R.L., McDonough, W.F., Cummings, M.L., 2013. Influence of chemical weathering on the composition of the continental crust: insights from Li and Nd isotopes in bauxite profiles developed on Columbia River basalts. Geochim. Cosmochim. Acta 115, 73–91.
Liu, X.M., Wanner, C., Rudnick, R.L., McDonough, W.F., 2015. Processes controlling δ7Li in rivers illuminated by study of streams and groundwaters draining basalts. Earth Planet. Sci. Lett. 409, 212–224.
Lyubartsev, A.P., Laasonen, K., Laaksonen, A.D., 2001. Hydration of Li+ ion. An ab initio molecular dynamics simulation. J. Chem. Phys. 114, 3120–3126.
Ma, T., Weynell, M., Li, S.L., Liu, Y., Chetelat, B., Zhong, J., Xu, S., Liu, C.Q., 2020. Lithium isotope compositions of the Yangtze River headwaters: weathering in high-relief catchments. Geochim. Cosmochim. Acta 280, 46–65.
Mainstone, C.P., Parr, W., 2002. Phosphorus in rivers—ecology and management. Sci. Total Environ. 282, 25–47.
Manning, B.A., Goldberg, S., 1997. Adsorption and stability of arsenic (III) at the clay mineral − water interface. Environ. Sci. Technol. 31, 2005–2011.
Miller, D.G., Ting, A.W., Rard, J.A., Eppstein, L.B., 1986. Ternary diffusion coefficients of the brine systems NaCl (0.5 M)-Na2SO4 (0.5 M)-H2O and NaCl (0.489 M)-MgCl2 (0.051 M)-H2O (seawater composition) at 25° C. Geochim. Cosmochim. Acta 50, 2397–2403.
Millot, R., Girard, J.P., 2007. Lithium isotope fractionation during adsorption onto mineral surfaces. International Meeting on Clays in Natural & Engineered Barriers for Radioactive Waste Confinement, Lille, France.
Millot, R., Vigier, N., Gaillardet, J., 2010. Behaviour of lithium and its isotopes during weathering in the Mackenzie Basin,Canada. Geochim. Cosmochim. Acta 74, 3897–3912.
Misra, S., Froelich, P.N., 2012. Lithium isotope history of cenozoic seawater: changes in silicate weathering and reverse weathering. Science 335, 818–823.
Nikanorov, A.M., Brazhnikova, L.V., 2009. Water chemical composition of rivers, lakes and wetlands. In: Khublaryan, M.G. (Ed.), Types And Properties of Water. vol. 2. EOLSS Co. Ltd., pp. 42–80 (Available at http://www.eolss.net/sample-chapters/c07/e2-03.pdf (December 2015)).
Olu-Owolabi, B.I., Unuabonah, E.I., 2011. Adsorption of Zn2+ and Cu2+ onto sulphate and phosphate-modified bentonite. Appl. Clay Sci. 51, 170–173.
Penniston-Dorland, S., Liu, X.M., Rudnick, R.L., 2017. Lithium isotope geochemistry. Rev. Mineral. Geochem. 82, 165–217.
Persson, I., 2010. Hydrated metal ions in aqueous solution: how regular are their structures? Pure Appl. Chem. 82, 1901–1917.
Pistiner, J.S., Henderson, G.M., 2003. Lithium-isotope fractionation during continental weathering processes. Earth Planet. Sci. Lett. 214, 327–339.
Pogge von Strandmann, P.A., Frings, P.J., Murphy, M.J., 2017a. Lithium isotope behaviour during weathering in the Ganges Alluvial Plain. Geochim. Cosmochim. Acta 198, 17–31.
Pogge von Strandmann, P.A., Desrochers, A., Murphy, M., Finlay, A., Selby, D., Lenton, T., 2017. Global climate stabilisation by chemical weathering during the Hirnantian glaciation. Geochem. Perspect. Lett. 3, 230–237.
Pogge von Strandmann, P.A., Kasemann, S.A., Wimpenny, J.B., 2020. Lithium and lithium isotopes in Earth's surface cycles. Elements 16, 253–258.
Pogge von Strandmann, P.A.P., Fraser, W.T., Hammond, S.J., Tarbuck, G., Wood, I.G., Oelkers, E.H., Murphy, M.J., 2019. Experimental determination of Li isotope behaviour during basalt weathering. Chem. Geol. 517, 34–43.
Rempe, S.B., Pratt, L.R., Hummer, G., Kress, J.D., Martin, R.L., Redondo, A., 2000. The hydration number of Li+ in liquid water. J. Am. Chem. Soc. 122 (5), 966–967.

Schauble, E.A., 2004. Applying stable isotope fractionation theory to new systems. Rev. Mineral. Geochem. 55, 65–111.
Sun, H., Gao, Y., Xiao, Y., Gu, H.O., Casey, J.F., 2016. Lithium isotope fractionation during incongruent melting: constraints from post-collisional leucogranite and residual enclaves from Bengbu uplift, China. Chem. Geol. 439, 71–82.
Tabor, N.J., Montanez, I.P., Southard, R.J., 2002. Paleoenvironmental reconstruction from chemical and isotopic compositions of Permo-Pennsylvanian pedogenic minerals. Geochim. Cosmochim. Acta 66, 3093–3107.
Tomascak, P.B., Magna, T., Dohmen, R., 2016. Advances in Lithium Isotopes Geochemistry. Springer-Verlag, Berlin.
Tournassat, C., Ferrage, E., Poinsignon, C., Charlet, L., 2004. The titration of clay minerals: II. Structure-based model and implications for clay reactivity. J. Colloid Interface Sci. 273, 234–246.
Velde, B., Meunier, A., 2008. Fundamentals of clay mineral crystal structure and physicochemical properties. The origin of clay minerals in soils and weathered rocks. Springer, Berlin, Heidelberg, pp. 3–73.
Vigier, N., Decarreau, A., Millot, R., Carignan, J., Petit, S., France-Lanord, C., 2008. Quantifying Li isotope fractionation during montmorillonite formation and implications for the Li cycle. Geochim. Cosmochim. Acta 72, 780–792.
Wanner, C., Sonnenthal, E.L., Liu, X.M., 2014. Seawater δ7Li: a direct proxy for global CO2 consumption by continental silicate weathering? Chem. Geol. 381, 154–167.
Wanner, C., Bucher, K., von Strandmann, P.A.P., Waber, H.N., Pettke, T., 2017. On the use of Li isotopes as a proxy for water–rock interaction in fractured crystalline rocks: a case study from the Gotthard rail base tunnel. Geochim. Cosmochim. Acta 198, 396–418.
West, A.J., Galy, A., Bickle, M., 2005. Tectonic and climatic controls on silicate weathering. Earth Planet. Sci. Lett. 235, 211–228.
Wimpenny, J., Colla, C.A., Yu, P., Yin, Q.Z., Rustad, J.R., Casey, W.H., 2015. Lithium isotope fractionation during uptake by gibbsite. Geochim. Cosmochim. Acta 168, 133–150.
Xu, W., Zhu, J.M., Johnson, T.M., Wang, X., Lin, Z.Q., Tan, D., Qin, H., 2020. Selenium isotope fractionation during adsorption by Fe, Mn and Al oxides. Geochim. Cosmochim. Acta 272, 121–136.
Xu, W., Qin, H.B., Zhu, J.M., Johnson, T.M., Tan, D., Liu, C., Takahashi, Y., 2021. Selenium isotope fractionation during adsorption onto montmorillonite and kaolinite. Appl. Clay Sci. 211, 106189.
Xu, Z., Li, T., Li, G., Hedding, D.W., Wang, Y., Gou, L.F., Zhao, L., Chen, J., 2022. Lithium isotopic composition of soil pore water: responses to evapotranspiration. Geology 50, 194–198.
Zhang, F., Dellinger, M., Hilton, R.G., Yu, J., Allen, M.B., Densmore, A.L., Sun, H., Jin, Z., 2022. Hydrological control of river and seawater lithium isotopes. Nat. Comm. 13, 1–10.
Zhang, W., Qi, L., Hu, Z., Zheng, C., Liu, Y., Chen, H., Gao, S., Hu, S., 2016. An investigation of digestion methods for trace elements in bauxite and their determination in ten bauxite reference materials using inductively coupled plasma-mass spectrometry. Geostand. Geoanal. Res. 40, 195–216.
Zhang, X.Y., Saldi, G.D., Schott, J., Bouchez, J., Kuessner, M., Montouillout, V., Henehan, M., Gaillardet, J., 2021. Experimental constraints on Li isotope fractionation during the interaction between kaolinite and seawater. Geochim. Cosmochim. Acta 292, 333–347.
Zhao, M.Y., Zheng, Y.F., 2015. The intensity of chemical weathering: geochemical constraints from marine detrital sediments of Triassic age in South China. Chem. Geol. 391, 111–122.